

**Radiation induced recombination centers in organic solar cells**

R. A. Street,\* J. E. Northrup, and B. S. Krusor

*Palo Alto Research Center, 3333 Coyote Hill Road, Palo Alto, California 94304, USA*

(Received 29 March 2012; published 25 May 2012)

Prolonged x-ray exposure of bulk heterojunction organic solar cells induces deep trap states that are observed in measurements of the photocurrent spectral response. The density of induced trap states is proportional to the density of recombination centers as measured by the voltage dependence of the photocurrent, therefore identifying the traps as primary recombination centers. The states are reversible by thermal annealing to about 100 °C, which implies a metastable structural change with binding energy 1–1.2 eV. However, the annealing kinetics reveal three different annealing processes, although for defect states with essentially the same electronic character. Analysis of the radiation damage indicates that defects are formed by hydrogen release from C-H bonds due to electronic excitation by the energetic secondary electrons created by the x rays. Theoretical structure calculations of possible hydrogen-related defects find specific defect states that match the experimental observations and provide values for hydrogen migration energies that are consistent with the annealing kinetics. The effects of prolonged white light exposure are very similar to x-ray exposure, although the annealing kinetics are significantly different. Measurements of the spectral response with bias illumination provide information about the energy level of the localized states.

DOI: [10.1103/PhysRevB.85.205211](https://doi.org/10.1103/PhysRevB.85.205211)

PACS number(s): 71.20.Rv, 73.50.Gr, 73.50.Pz, 73.20.Hb

**I. INTRODUCTION**

Bulk heterojunction (BHJ) organic solar cells degrade in performance by variable amounts under prolonged illumination.<sup>1,2</sup> In some cases the light induced changes are reversible by thermal annealing.<sup>3</sup> There has been considerable discussion as to whether the effects are related to the contact materials or to the active materials and whether the changes are intrinsic or impurity related.<sup>4–6</sup> Ambient exposure plays a significant role in cell stability, but fabrication of air-stable cells has greatly improved.<sup>7,8</sup> Organic light emitting diodes (OLED) also degrade in operation, although lifetimes have improved greatly over recent years, and reversible changes are also observed.<sup>9,10</sup> OLED degradation is associated with the light emission and may therefore have a similar mechanism to the solar cells. We report elsewhere that prolonged white light illumination creates deep states in the active layers of a BHJ solar cell and that these states act as recombination centers.<sup>11</sup> In order to understand the role of induced electronic defects in more detail, the effects of x-ray irradiation on BHJ solar cells are studied here. Radiation damage measurements provide insight into the nature of defects and their role in electronic transport and recombination. Ionizing radiation in semiconducting polymers has been well studied and provides quantitative information about defect creation.

The second reason for interest in the effects of radiation damage is that the BHJ structure is a possible photodiode structure for x-ray image sensors, and it is important to estimate the operational lifetime of such a device in a medical imaging application.<sup>12</sup> There is previous evidence that x-ray exposure leads to degradation of conjugated polymers and BHJ solar cells, but details of the nature of the damage effect have not been established.<sup>13–15</sup>

Experimental techniques to probe the localized state distribution through measurements of the photocurrent spectral response have been developed.<sup>16,17</sup> Optical excitations at energy below the interface band gap (the energy gap separating the donor valence band and the acceptor conduction band)

induce transitions from trap states to conducting states. The magnitude of the absorption as measured by the spectral response allows the relative density of states to be monitored, and the shape of the spectrum characterizes the type of localized state.<sup>11,16</sup>

Sec. II describes the measurement techniques and presents data from x-ray irradiated solar cells, annealing effects, and a comparison with light induced defects. Sec. III provides an approximate quantitative analysis of the radiation damage and a theoretical analysis of the electronic structure of plausible defect states. Sec. IV discusses various aspects of the measurements and the models for defect creation and annealing, and Sec. V presents the conclusions.

**II. MEASUREMENTS**

Most of the x-ray exposures were made on poly(carbazole-dithienyl-benzothiadiazole):phenyl C<sub>70</sub>-butyric acid methyl ester (PCDTBT:PC<sub>70</sub>BM) cells,<sup>18</sup> including cells in which the active layer is about 200-nm thick, roughly double the thickness of typical optimized solar cells. The samples are from the same set that our colleagues and ourselves have studied previously,<sup>19,20</sup> and the cell fabrication and structure are described elsewhere.<sup>21</sup> The increased thickness gives greater sensitivity to weak optical absorption from traps and also increases the x-ray absorption but results in a smaller fill factor than optimized cells so that the thicker cell efficiency is about 3.5%. One series of similar measurements was made with poly(3-hexyl thiophene) (P3HT):PCBM. Measurements of the photocurrent spectral response use a 224 Hz chopped monochromatic light source and a lock-in amplifier, as described previously.<sup>16</sup> The signal is normalized to the incident light intensity, which is of the order 0.1 mW/cm<sup>2</sup>. The measurements of the voltage dependence of the photocurrent use a white light source chopped at 80 Hz and lock-in detection to subtract the dark current. The dark diode characteristics are measured under quasi-steady state conditions.

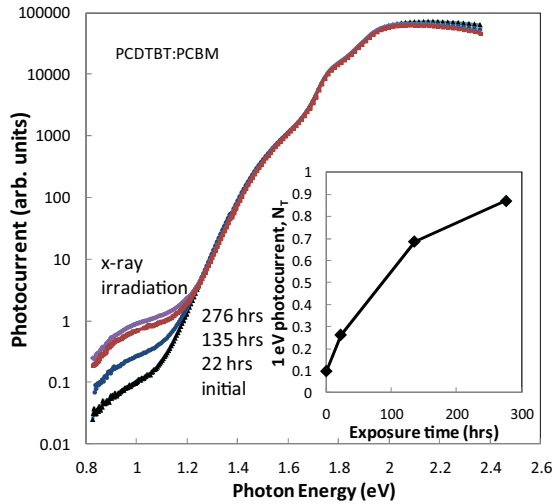


FIG. 1. (Color online) Photocurrent spectral response data for a PCDTBT:PCBM solar cell after various times of 8 keV x-ray irradiation as indicated. The data are normalized to the value at 1.8–2 eV. The inset shows the magnitude of the photocurrent signal measured at 1 eV as a function of the total x-ray exposure.

The devices are exposed to x rays from a Cu target operating at 40 kV. Most of the x-ray emission is in the  $K\alpha$  lines near 8 keV rather than in the Bremsstrahlung band. This energy is large enough to penetrate the thin cover glass encapsulation layer on the solar cell but low enough for significant absorption in the active layer—about  $30\times$  the absorption of 50 keV x rays, which is more typical of medical x-ray exposures. Hence this x-ray energy should give more damage than in typical x-ray use. The exposure dose was measured to be 1 cGy/s (1 R/s), which corresponds to about  $7\times 10^8$  x-ray photons/cm<sup>2</sup>/sec, and the transmittance through the encapsulation is estimated to be 30% from the known mass-absorption coefficients, so that the exposure at the active layer is about  $2\times 10^7$  x-ray photons/cm<sup>2</sup>/sec.

In one series of measurements three separate x-ray exposures were made of 22 hours, 113 hours, and 141 hours over a period of about 6 weeks. The total exposure of 276 hours ( $\sim 10^6$  s) at the completion of the experiments was therefore  $\sim 10^4$  Gy. Optical absorption measurements did not find any significant changes in the film as a result of the x-ray dose. The photocurrent spectral response after these x-ray exposures, measured at zero applied bias, is shown in Fig. 1. The peak response near 2 eV decreased by about 40% after the irradiation due to the change in the voltage dependence of the photocurrent, as discussed below, and the data are normalized to correct for this drop in overall sensitivity.

The photocurrent spectral response measures the product of the illumination intensity, the optical absorption at the measured wavelength, and the probability that an absorbed photon generates mobile charge. The spectrum therefore measures the optical absorption of those optical transitions that excite carriers to mobile states. As discussed elsewhere, photon energies above about 1.7 eV correspond to bulk absorption in the polymer or fullerene domains,<sup>16,22</sup> which generate conducting carriers by exciton diffusion to the domain boundary where it forms a weakly bound charge transfer (CT)

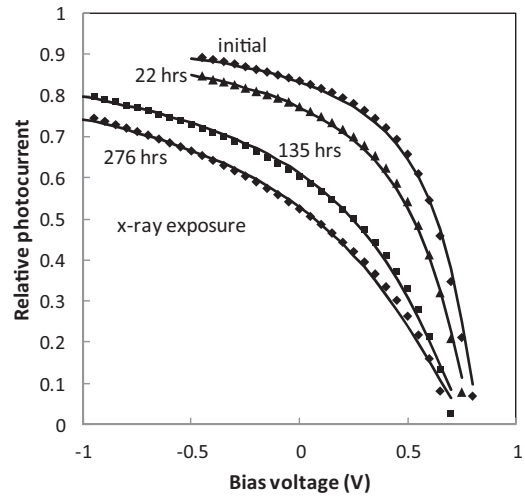


FIG. 2. Voltage dependence of the photocurrent for the initial state and after x-ray exposure, for the sample of Fig. 1. The solid line is a model fit from which the mobility-lifetime product is extracted.

state and separates into conducting electrons and holes. The energy below about 1.7 eV corresponds to direct excitation of the CT state.<sup>23,24</sup> The exponential decrease below about 1.4 eV reflects CT transitions that involve the exponential band tail to the density of states, believed to arise predominately from the disorder in the polymer domain.<sup>16</sup> The broad band below 1.2 eV is due to optical excitation of much deeper trap states extending well into interface band gap. Other studies have found evidence for trap states in BHJ solar cells.<sup>25–27</sup>

Figure 1 shows clearly that the dominant effect of x-ray irradiation is a large increase in absorption in the low energy range. Since the absorption is proportional to the density of states, the data indicate that there is a corresponding increase in the deep trap density. There is no discernible change in the slope of the exponential absorption or the shape of the higher energy CT absorption. Above 2.3 eV there is a small reduction in signal relative to the peak, which we attribute to a relative reduction in cell efficiency for highly absorbed light. As discussed further below, the low energy optical transitions must excite both electrons and holes from the deep trap states to mobile conducting states in order to induce steady state photoconductivity.

Since the low energy absorption band does not change shape with irradiation, the relative trap density is obtained from the magnitude of the absorption at a convenient energy within the band, which we choose to be 1 eV. The relative deep trap concentration  $N_T$ , as measured by the response at 1 eV, increases with x-ray exposure, as shown in the inset to Fig. 1. There is a sublinear dependence on exposure indicating a gradual saturation. In this sample and all others measured, the low energy band in the spectral response is present before the irradiation.

The increase in  $N_T$  is accompanied by corresponding changes to the electrical characteristics of the cells, as shown in Fig. 2. The voltage dependence of the photoconductivity  $J_{PC}(V)$  becomes weaker with increased exposure, corresponding to a reduction in fill factor and demonstrating that there is increased recombination.  $J_{PC}(V)$  is measured with light intensity varying from about 0.5–100 mW/cm<sup>2</sup>. The measurements

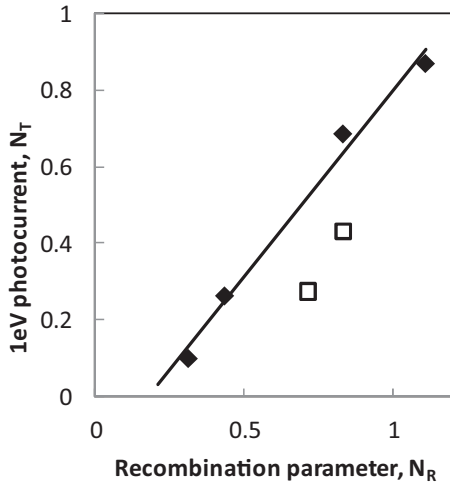


FIG. 3. A plot of the relation between the trap density  $N_T$ , as measured by the 1 eV photocurrent, and the recombination center density  $N_R$ , as measured by the voltage dependence of the photocurrent. Closed symbols are for data resulting from x-ray exposure, and open symbols are data as a result of annealing.

at 10 mW/cm<sup>2</sup> and below are independent of intensity and are used to extract the recombination, as the higher intensity data can be influenced by series resistance<sup>28,29</sup> or bimolecular recombination. The solid lines in Fig. 2 are fits to  $J_{PC}(V)$  of a model used previously, in which the shape is determined by the mobility-lifetime ( $\mu\tau$ ) product of the mobile charge.<sup>30</sup> The basis of the model is that the carrier moves a distance  $\mu\tau F$  before recombination, where  $F$  is the electric field, and this value relative to the device thickness determines the probability of recombination. According to standard models for localized states with a capture cross-section  $\sigma$ , the density of recombination centers,  $N_R$ , is inversely proportional to  $\mu\tau$ ,<sup>11,30</sup>

$$\mu\tau = \text{const}/\sigma N_R. \quad (1)$$

This analysis of trapping is based on the  $\mu\tau$  product and does not provide information about the separate changes in  $\mu$  and  $\tau$ . The relative value of  $N_R$  is therefore obtained from (1) and the data of Fig. 2. Figure 3 shows that there is a linear relation between  $N_T$  and  $N_R$ , which is clear evidence that the trap states observed in the spectral response absorption are the recombination centers influencing the cell properties. As we point out elsewhere, the residual recombination when the trap density tends to zero is due to an alternative recombination channel through band tail states.<sup>11</sup> Measurements were also made of the dark forward bias current after each x-ray exposure. The exponential diode region exhibits an increase in ideality factor from 2 to 3.5, as shown in Fig. 4, and an increase in the series resistance. The initial ideality factor is larger than in thinner solar cells of the same material.<sup>11,30,31</sup> The diode forward current is controlled by recombination, and the increased ideality factor is another manifestation of the recombination through deep traps.<sup>32,33</sup> Similar spectral response,  $J_{PC}(V)$ , and ideality factor changes as a result of prolonged white light illumination are reported separately.<sup>11</sup>

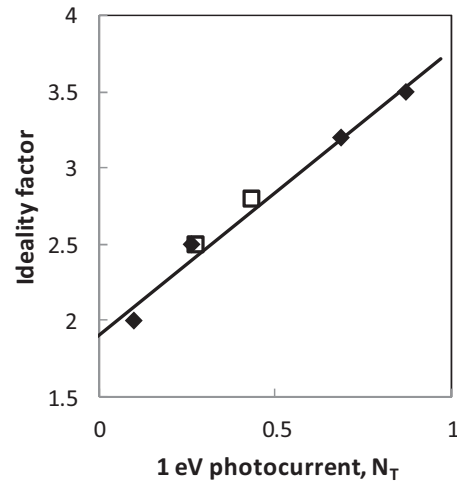


FIG. 4. A plot of the dark diode forward current ideality factor versus the trap density  $N_T$  as measured by the 1 eV absorption strength. Closed symbols are for data resulting from x-ray exposure, and open symbols are data as a result of annealing.

#### A. Spectral response measurements with bias light

Measurements of the spectral response with a steady state bias light were made to provide further information about the optical transitions through the trap states. The bias light was provided by a red light-emitting diode with a wavelength of 650 nm, but aside from this illumination the spectral response measurement is made exactly as before. The illumination above the main absorption band allows the spectral response measurement to be made under conditions of greatly increased optical excitation. The optical excitation changes the occupancy of both the transport and the trap states and can therefore affect the spectral response. Figure 5 shows the spectral response data for a second PCDTBT:PCBM

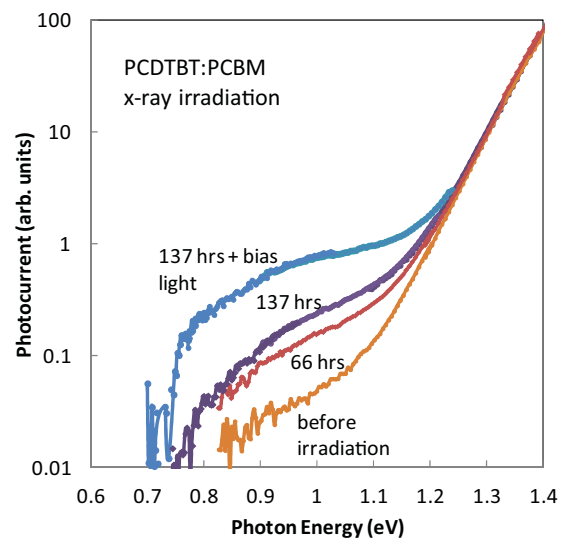


FIG. 5. (Color online) Photocurrent spectral response data for a second PCDTBT:PCBM solar cell after two x-ray irradiations for the times indicated. The data are normalized to the value at 1.8–2 eV. The spectral response of the fully irradiated sample measured with red bias light illumination is also shown.

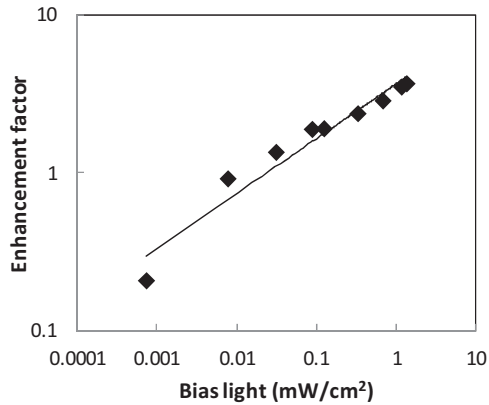


FIG. 6. Plot of the photocurrent enhancement factor induced by bias light illumination versus the bias light intensity.

sample subject to x-ray irradiation for 66 hours and 137 hours. The irradiation results are very similar to the sample of Fig. 1. Figure 5 also shows that the low energy trap-related spectral response signal is increased as a result of the bias light measurement, while no significant change is observed at higher energy. The increase with bias light is also present in the low energy band of the sample before irradiation. The relative increase is about a factor 2 for the unexposed sample and grows to 3.3 after 137 hours of irradiation. Similar bias light enhancement is found for samples subject to prolonged white light illumination, as discussed further below.

Figure 6 shows how the signal enhancement depends on the intensity of the bias illumination for an irradiated sample. The enhancement is defined as the ratio of the increase in response with bias light to the signal without bias light. The enhancement increases roughly as the  $1/3$  power of the bias light intensity and reaches an enhancement factor of about 4 at an illumination level of  $\sim 1$   $\text{mW}/\text{cm}^2$ . Since the bias light is highly absorbed compared to excitation at 1 eV, it generates about  $10^5$  times more mobile carriers. The larger photocurrent in the bias light measurement increases the signal-to-noise and allows measurements to lower energy. The data in Fig. 5 shows that the low energy absorption band cuts off relatively abruptly at 0.7–0.75 eV for the irradiated state with and without bias light.

### B. Defect annealing and recovery

After the final x-ray exposure the sample of Fig. 1 was stored in nitrogen and then remeasured after 30 days. The deep trap absorption band decreased slightly relative to the other regions of the spectrum, indicating a relaxation in the trap density. The sublinear dependence of the induced trap density, with dose shown in the inset to Fig. 1, may therefore have a contribution from partial recovery between measurements. Subsequently the sample was annealed in air at 60 °C for 3 hours, 88 °C for 2 hours, and 108 °C for 80 minutes. The low energy spectral response in Fig. 7 and the annealing data in Fig. 8 show that the states introduced by the x-ray damage are reversible and are removed by annealing. The highest anneal temperature of 108 °C is close to the temperature at which morphological changes occur, and so higher temperatures and/or longer anneal times were not

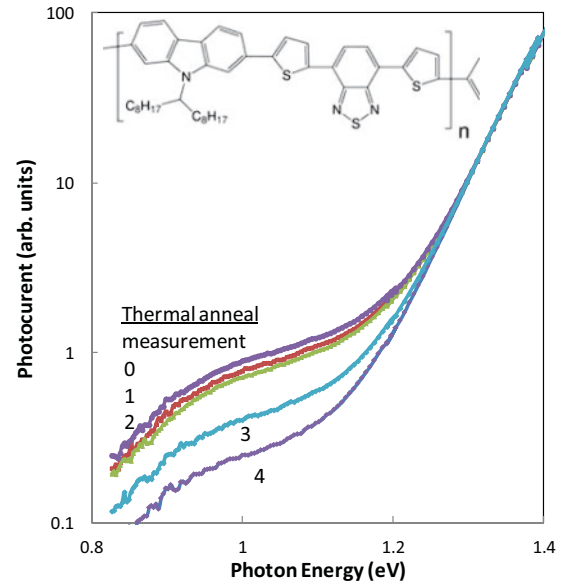


FIG. 7. (Color online) Photocurrent spectral response data for the PCDTBT:PCBM solar cell of Fig. 1, after various stages of thermal annealing. Data measurements: (0) shortly after the final x-ray exposure; (1) rested at room temperature for 30 days; (2) annealed at 60 °C for 3 hours; (3) annealed at 88 °C for 2 hours; (4) annealed at 108 °C for 80 minutes. The atomic structure of PCDTBT is also shown.

attempted in this series of measurements. After this final anneal, the low energy absorption band has decreased to 25% of the strength immediately after the last x-ray exposure and is about twice the magnitude of the absorption before the start of the x-ray exposure.

In order to obtain more detailed information about the annealing kinetics, the sample of Fig. 5 was also annealed after the x-ray irradiation. In this case the annealing temperature was held constant at 85 °C, and the spectral response was measured after annealing times from 30 minutes to 200 hours. The corresponding low energy spectra in Fig. 9 show details of the

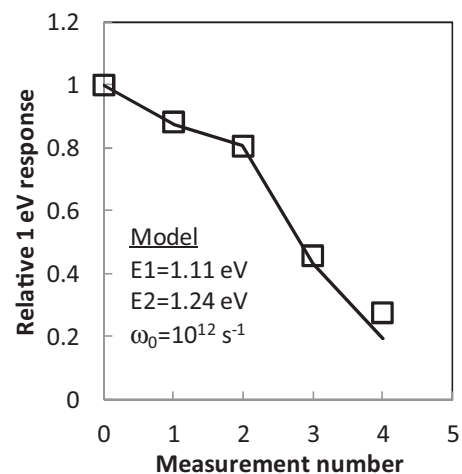


FIG. 8. Plot of the strength of the 1 eV photocurrent after the various stages of annealing shown in Fig. 7 (open data points), compared to the model (line) described in the text. The measurement numbers are those in Fig. 7.

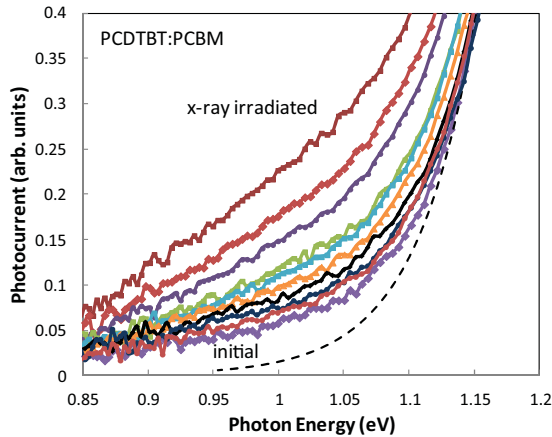


FIG. 9. (Color online) Spectral response data for the PCDTBT:PCBM sample of Fig. 5 immediately after irradiation (top curve) and after sequential annealing steps at 85 °C. The annealing times are 0.5, 1.25, 3.1, 6.25, 21.7, 45.2, 141, and 212 hours. The lowest data set is the measurement before irradiation, and the dashed line is an extrapolation of the exponential band tail absorption region of the spectral response. Note the linear photocurrent scale.

annealing, and the relative response at 1 eV is shown in Fig. 10 as a function of the anneal time. The intensity of the low energy absorption band drops by about 50% after 2–3 hours anneal but then decreases much more slowly, eventually returning to the value before the irradiation after more than 200 hours of annealing.

Annealing also recovers the electrical performance of the cells, as shown in Figs. 3 and 4 for the sample of Fig. 1.  $N_R$  derived from  $J_{PC}(V)$  recovers but does not exactly follow the trend during exposure, suggesting that there is some additional recombination that does not anneal out. The ideality factor recovery almost exactly matches the trend observed during the exposure. For the sample of Fig. 5 the value of  $N_R$  derived from

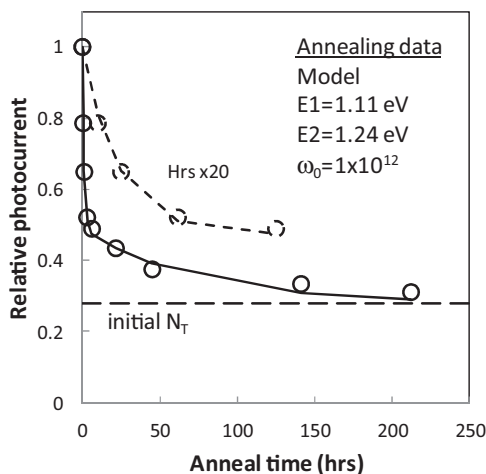


FIG. 10. Plot of the relative photocurrent measured at 1 eV as a result of annealing the sample of Fig. 9 at 85 °C for various times. The lines are a fit to a model described in the text, and the model parameters are indicated. The dashed data and line has a 20-fold expansion of the time scale to show the faster annealing process more clearly. The horizontal dashed line represents the photocurrent signal before irradiation.

$J_{PC}(V)$  also does not recover completely and is about 30% larger than the initial data. In this sample the ideality factor also does not fully recover, ending at 1.75 compared to the initial 1.65, and we also find that the band tail region of the spectral response data (energy range 1.2–1.4 eV) broadens slightly, from 44.2 to 45.9 meV. These changes are all consistent with slightly increased band tail recombination, possibly due to slight morphological changes after the long anneal, since they follow the trend that we have observed for much higher temperature but shorter anneals.<sup>11</sup>

The annealing of the low energy spectrum evidently reflects a thermally activated process, and hence the time  $t$  and temperature  $T$  dependence of the relaxation of the absorption intensity  $I_A$  is described by the usual relations,

$$I_A = I_0 \exp(-t/\tau); \quad \tau = \omega_0^{-1} \exp(E/kT), \quad (2)$$

where  $E$  is the activation energy and  $\omega_0$  is the rate prefactor. The initial faster decay followed by a much slower decay in the constant temperature data of Fig. 9 suggests two different time constants, and the solid line in Fig. 10 shows a good fit to the following model,

$$I_A/I_0 = C_0 + C_1 \exp(-t/\tau_1) + C_2 \exp(-t/\tau_2). \quad (3)$$

The parameters for the faster decay are  $C_1 = 0.51$ ,  $\tau_1 = 1.1$  hrs; for the slower decay  $C_2 = 0.21$ ,  $\tau_2 = 70$  hrs. The initial signal has parameter  $C_0 = 0.28$ . Assuming  $\omega_0 = 10^{12} \text{ s}^{-1}$  gives the corresponding activation energies of  $E_1 = 1.11$  and  $E_2 = 1.24$  eV. The prefactor cannot be determined accurately from the measurements, and changing the prefactor by  $10 \times$  gives similar results but with the activation energies changed by about 0.08 eV. The solid line in Fig. 8 shows that the calculated recovery for the data in Fig. 7 is a good fit to the data using a model of the same two time constants and an initial response that does not anneal out. The data therefore indicate that there are more than one distinct annealing processes and provide estimates of the energy associated with the annealing processes.

### C. Light induced defects

The x-ray damage reported here is similar to the effects of prolonged light exposure in PCDTBT:PCBM cells.<sup>11</sup> After light exposure, there is a similar increase in the photocurrent spectral response in the 0.8–1.2 eV energy region but no significant change in the other regions of the spectrum, as shown in Fig. 11. Bias light results in an enhancement of the low energy spectrum, as observed for the x-ray irradiated samples. Quantitatively similar changes in  $J_{PC}(V)$  and in the dark current ideality factor are observed.

Similar annealing studies to those of the x-ray irradiated samples were conducted to characterize further the effects of light exposure, and the results are also shown in Fig. 11. First the device was remeasured about four months after the light induced defects were created, and no discernible change in the signal was found. Then the sample was annealed at 97 °C for 2 hours, at 104 °C for 4.6 hours, and then a series of measurements at 92 °C for anneal times extending to 332 hours. The first of these measurements reduced the low energy signal by about 20%, the second by a further 10%, and the 92 °C anneal continued to reduce the signal,

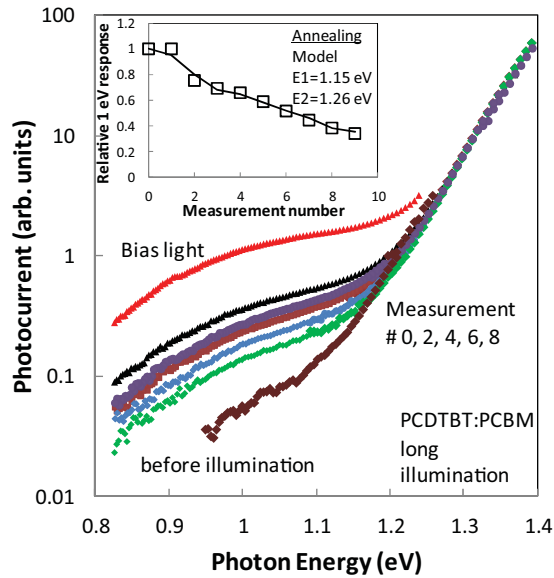


FIG. 11. (Color online) The spectral response of a PCDTBT:PCBM sample after prolonged exposure to white light, showing the effects of thermal annealing and bias light illumination. The insert shows the various annealing steps (open symbols) and the prediction of the annealing model described in the text, with the parameters indicated. Annealing times at 92 °C are 8, 24, 48, 77, 165, and 332 hours (measurement #4–9).

so that after 332 hours it was  $\sim 35\%$  of the value immediately after the illumination and showing no further annealing effect. Evidently the light induced states are partially reversible, but the rapid annealing found for x-ray exposure is much reduced and there is a larger residual stable state. To compare the annealing properties of the two types of exposure, the inset in Fig. 11 shows the predicted result of annealing using the same model as for the data in Fig. 6, with faster and slower anneal processes and a stable baseline. The fast and slow annealing processes account for the extended time measurements but with slightly larger activation energies (1.15 and 1.26 eV) than for the x-ray irradiated sample (assuming the same value of  $\omega_0$ ). The model suggests that about 20% of the original signal anneals out with the faster time constant, 45% with the slower time constant, and the remaining 35% is stable at this anneal temperature. Evidently x-ray induced and light induced recombination centers are broadly similar but have some different characteristic annealing properties. Further detailed measurements are needed to explore the light induced defect creation and annealing kinetics more completely.

#### D. X-ray irradiation of P3HT solar cells

X-ray irradiation measurements were also made on P3HT:PCBM solar cells to see if the properties found for PCDTBT:PCBM were common to other organic solar cells. Figure 12 shows the photocurrent spectral response of one device before and after 91.5 hours of irradiation as well as the effects of annealing. The spectral response of the nonirradiated device shows generally the same features as for PCDTBT:PCBM. The CT absorption extends from 1.7 to about 1 eV due to the lower interface band gap, with the exponential band tail region occurring between 0.9 and 1.1 eV.<sup>16</sup> There is

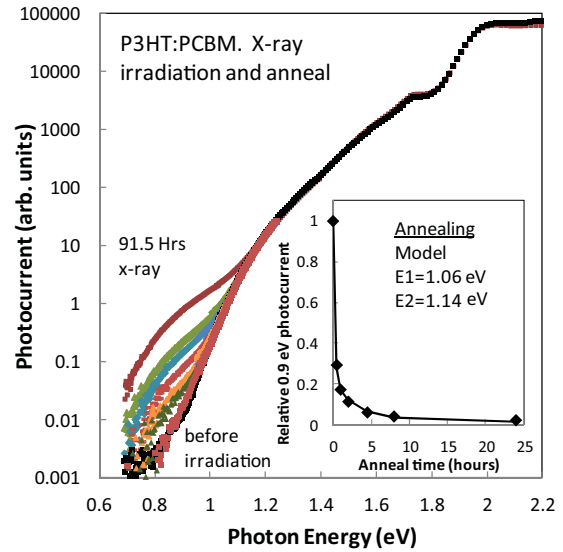


FIG. 12. (Color online) The spectral response of a P3HT:PCBM solar cell before and after x-ray irradiation and at various stages of annealing at 85 °C for total times of 0.5, 1.0, 2.0, 4.5, 8, and 24 hours. The 24 hours data is virtually coincident with the data before irradiation. The inset shows the relative photocurrent, measured at 0.9 eV as a function of annealing time. Points are the data, and the line is a fit to the annealing model with the parameters indicated.

a broader band at lower energy (below 0.9 eV), qualitatively similar to the low energy region in PCDTBT:PCBM. X-ray irradiation induces a large increase in the low energy band but no significant change in the other regions of the spectrum, apart from an overall decrease in photocurrent by about 50% associated with the relative reduction of  $J_{PC}(V)$  at zero bias. The data in Fig. 12 are scaled so that the higher energy regions overlap, as was done for the PCDTBT samples. Measurements with a red bias light found a smaller enhancement of only 40–50% in the low energy band.

The dc photocurrent  $J_{PC}(V)$  changes in the same manner as the Fig. 2 data for PCDTBT:PCBM, with a weaker dependence on voltage due to increased recombination. Evaluation of the shape of  $J_{PC}(V)$  according to Eq. (1) indicates a sixfold increase in the density of recombination centers. In addition the dark current exhibits an increase in ideality factor, although a low shunt resistance in this device does not allow a very accurate measurement.

The annealing effects are also broadly similar to PCDTBT:PCBM. Figure 12 shows the spectral response after several annealing times at a temperature of 85 °C, and the inset to the figure shows a plot of the photocurrent measured at 0.9 eV as a function of the annealing time. Annealing reduces the photocurrent response rapidly first and then more slowly, and after 24 hours anneal there is complete recovery to the signal acquired before the irradiation. The solid line is a fit to the same model as for PCDTBT:PCBM, with two time constants (0.25 and 3.5 hours) and the constant background. The initial fast decay is more pronounced than that measured for PCDTBT:PCBM and accounts for about 80% of the recovery. The two time constants are smaller than for PCDTBT:PCBM and correspond to energies  $E_1 = 1.06$  eV and  $E_2 = 1.14$  eV assuming the same value of  $\omega_0$ . The ideality

factor and  $J_{PC}(V)$  fully recover their initial values. Overall the two types of solar cell exhibit a very similar response to x-ray irradiation and annealing.

### III. DEFECT STATE ANALYSIS

#### A. Quantification of the radiation damage

X-ray absorption creates high energy electrons by the photoelectric effect, and these electrons lose energy by ionization that creates secondary electron-hole pairs. The typical secondary electron-hole energy is a few times the band gap and hence 5–20 eV. Ultraviolet (UV) light is the same energy range, and it is well known that polymers exhibit substantial UV damage, so it is natural to associate the x-ray damage with the energetic secondaries. A minimum energy of about 4 eV is required to break a C-C or C-H bond, which is therefore well within this energy range. The photoelectron can also lose energy by a displacement collision with an atom nucleus, but the large difference in the electron and nuclear mass limits the possible energy transfer and the mechanism is not significant at the x-ray energy used.

There have been several detailed studies on the effect of radiation on organic semiconductors, particularly P3HT, which are very helpful in quantifying the effects. Comparable damage effects can be expected in PCDTBT, which, like P3HT, contains both alkyl chains and thiophenes, although an additional damage effect associated with the nitrogen bonds is possible but not likely. Since the x-ray effect arises from the secondary electrons, the same damage is expected for x-ray or high-energy electron exposure and reasonably independent of the radiation energy. Extensive radiation damage of P3HT breaks C-H bonds, releases sulphur, and produces cross-linking and eventually graphitization, but these effects are observed after orders of magnitude more exposure than in our measurements.<sup>34,35</sup> At lower exposures, but still exceeding ours, the only effect found was the breaking of C-H bonds and the associated release of hydrogen.<sup>36</sup> Less is known about radiation damage to fullerenes; one study of C60 finds structural damage but after much higher exposure than P3HT.<sup>37</sup> PCBM contains a few C-H bonds which presumably can break under irradiation, but possibly the damage effects are predominately in the polymer.

These literature studies allow us to estimate the damage induced defect density by estimating the number of broken C-H bonds. Bebensee *et al.* report that an exposure of  $7 \times 10^{15}$  e/cm<sup>2</sup> of 100 eV electrons causes hydrogen abstraction from about 50% of the carbon atoms in the exposed P3HT layer.<sup>36</sup> One hundred eV electrons have a mean free path of about 10Å, and each electron should result in about 10 secondary electrons. The density of C-H bonds in P3HT is about  $5 \times 10^{22}$  cm<sup>-3</sup> and leads to an estimate that approximately 1% of the secondary electrons induce C-H bond breaking.

The radiation exposure in our measurements of  $2 \times 10^7$  x-ray photons/cm<sup>2</sup>/sec, corrected for the absorption in the encapsulation, and the exposure time of  $10^6$  sec gives a total exposure of  $2 \times 10^{13}$  x-ray photons/cm<sup>2</sup> for the sample of Fig. 1. The calculation of the secondary electron density is complicated by the presence of the encapsulation layer, but

from the known x-ray attenuation of glass and polymers and the stopping power of the photoelectrons we estimate  $1-2 \times 10^{19}$  cm<sup>-3</sup> of secondary electrons. Applying the 1% damage estimate indicates about  $1-2 \times 10^{17}$  cm<sup>-3</sup> broken C-H bonds, which we equate with the total defect density. Only states close to the heterojunction interface act as recombination centers because recombination involves transitions to both the polymer valence band and the fullerene conduction band. Previously we have estimated that if the localized states are distributed uniformly, then about 10% are close enough to the interface to be recombination centers. Hence the estimate reduces to a recombination center density of  $\sim 1-2 \times 10^{16}$  cm<sup>-3</sup>. The role of the defect states that are not near the interface is discussed further below. Clearly these estimates are highly approximate but give a reasonable order of magnitude. Long time transient photoconductivity (TPC) has been used to measure the deep trap density, and values of  $\sim 5 \times 10^{16}$  cm<sup>-3</sup> were found for PCDTBT:PCBM cells not subject to irradiation.<sup>38</sup> The TPC experiment is sensitive to all the traps not just the recombination centers near the heterojunction interface, and so the values are reasonably consistent.

#### B. Theoretical analysis of defect energetics

The radiation damage analysis indicates that the trap states are a result of hydrogen release from C-H bonds. First principles density functional pseudopotential calculations<sup>39-41</sup> were therefore performed to determine the electronic properties and energetics of hydrogen-related defects in poly-3-alkylthiophene (P3AT). In particular we examine defects which may be created by transferring H atoms from alkyl-chains to the conjugated polymer backbone. Atomic structure and total energy calculations were performed within the local density functional theory, as discussed in previous calculations for thiophenes<sup>42</sup> and polyacenes.<sup>43</sup> A plane wave basis is employed with a cutoff energy of 40 Ry. Calculations were performed for both isolated polymers and bulk systems. The length of the repeating unit along the polymer backbone was varied between four and eight S atoms.

A possible explanation for the origin of the gap states in irradiated P3HT involves defects created by breaking a C-H bond in the alkyl-chain or on the thiophene rings and adding the removed H atom to a C atom in the conjugated backbone. Approximately 4–5 eV is required to break a C-H bond. It is therefore likely that irradiation by x rays may break C-H bonds in the alkyl chain region of an organic material. This would result in the creation of a free radical defect in which a C atom in the alkyl chain, which was previously fourfold coordinated, now has two C-C bonds and one C-H bond. We refer to such a free radical defect as a hydrogen vacancy  $V_H$ . Atomic relaxation will occur so that the C atom becomes sp<sup>2</sup> coordinated with a singly occupied  $2p$  orbital. The structure of a  $V_H$  defect is illustrated in Fig. 13. H atoms freed by the irradiation may attach to a C atom in the conjugated chain, thereby giving rise to overcoordinated C atoms. One such defect, a CH<sub>2</sub> defect, is shown in Fig. 14.

##### (1) Hydrogen vacancies

The preferred location for a hydrogen vacancy in the alkyl chain was determined by calculating total energies for  $V_H$  on each of the sites on the alkyl chain, as shown in

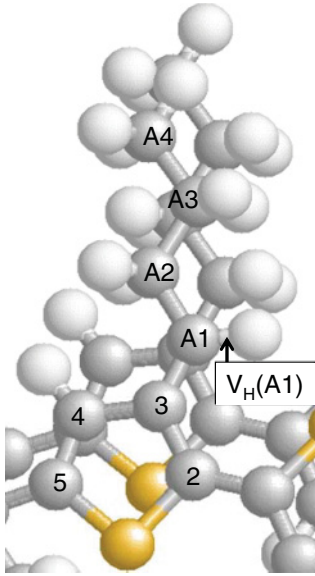


FIG. 13. (Color online) An atomic model of a segment of P3AT is shown with a 4-atom alkyl chain. Atom A1 is bonded to only one H atom, thus there is a hydrogen vacancy ( $V_H$ ) on atom A1.

Fig. 13. These calculations predict that the  $V_H$  prefers to reside on the carbon atom that is nearest to the conjugated chain. Referring to nomenclature defined in Fig. 13 we find  $V_H(A1)$  is lower in energy than  $V_H(A2)$ ,  $V_H(A3)$ , and  $V_H(A4)$  by 0.9 eV. This preference for  $V_H(A1)$  is understood as arising from the increase in  $\pi$ -bonding interaction afforded by having the  $sp^2$  carbon next to the conjugated chain. Such a preferred location is likely to be a general result for organic semiconductors comprising  $\pi$ -bonded cores and attached alkyl chains, e.g., 2,9-dialkyl-dinaphtho[2,3-b:2',3'-f]thieno[3,2-b]thiophene (DNTT), and poly(2,5-bis(3-tetradecylthiophen-2-yl)thieno[3,2-b]thiophene) (PBTBT). It is possible for a hydrogen vacancy to form on the C atom that is next to the nitrogen atom in PCDTBT. The alkyl chains in PCDTBT are separated from the conjugated ring by the nitrogen atom, and hence in this material the energy preference for forming hydrogen vacancies adjacent to the conjugated chain may be smaller than in P3AT.

Calculations of the migration energy for  $V_H$  in the alkyl chain were performed with a simplified model wherein the chain is attached to a single thiophene ring. The vacancy

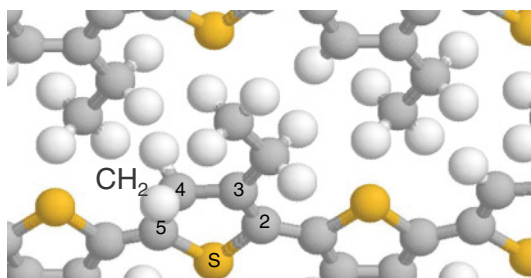


FIG. 14. (Color online) An atomic model of a  $CH_2$  defect is shown, in which the added H atom is located on C atom 4. It is also possible to place the extra H atom on atoms 2, 3, 5, or on the S atom, but these structures have higher energy.

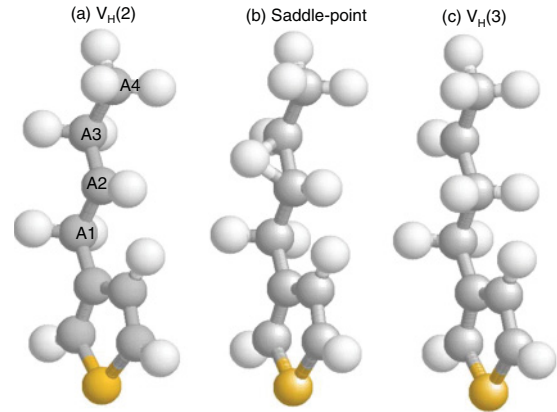


FIG. 15. (Color online) An atomic model showing a possible path for migration of  $V_H$  along an alkyl chain. (a) Indicates  $V_H(A2)$ , (b) indicates a saddle-point configuration, and (c) depicts  $V_H(A3)$ . The vacancy migrates from A2 to A3 by moving a hydrogen atom from A3 to A2.

migrates from carbon number  $n$  to  $n - 1$  by migration of an H atom from  $n - 1$  to  $n$ . An initial state, an intermediate saddle-point structure, and the final state are shown in Fig. 15. Calculations show that the energy of the saddle-point configuration exceeds the energy of the initial state by 1.4 eV. This result for the activation energy for migration of the  $V_H$  along the alkyl chain is probably an overestimate because quantum mechanical tunneling of the proton over short distances is not taken into account.

(2) Additional H atoms on the conjugated chain:  $CH_2$  defects

Calculations were performed for the possible structures obtained by bonding an additional H atom to the conjugated chain. Such defects would arise if H atoms that were knocked out of a nearby alkyl chain rebounded to a conjugated chain. The most stable configuration is the one shown in Fig. 14, which illustrates a defect where the added H atom is bonded to C atom number 4. This structure will be denoted a  $CH_2$  defect, similar to those studied for pentacene.<sup>43</sup> It is also possible to add the H to C atoms 2, 3, 5, or to the S atom. The relative energies of the five possibilities were calculated. The  $CH_2$  defect, with the H on C atom 4, is predicted to be more stable than the other four possibilities. The relative energies are  $\Delta E(5) = 0.33$  eV,  $\Delta E(2) = 0.35$  eV,  $\Delta E(3) = 0.31$  eV, and  $\Delta E(S) = 1.35$  eV. The last value shows that it is highly unlikely that an S-H defect forms.

Migration of H along the conjugated P3HT backbone may occur along a path connecting 2-3-4-5. Calculations indicate that the energy required for H migration along the backbone is  $\sim 1.2$  eV. A saddle point configuration between sites 2 and 5 is shown in Fig. 16. In addition it is possible for a  $CH_2$  defect to migrate from one polymer chain to a neighbor. The activation energy for this process was found to be 0.7 eV, and the saddle point geometry, where the H atom is midway between the two polymers, is shown in Fig. 17. The low activation energy implies that hydrogen can migrate well away from the original molecule.

It is likely that defects created by x-ray irradiation can be annealed out by recombination of an H atom migrating along the

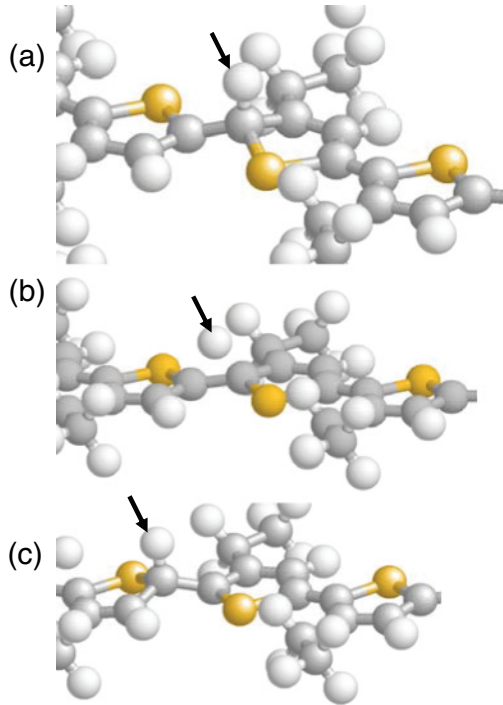


FIG. 16. (Color online) An atomic model showing a possible path for migration of an H atom along the conjugated backbone. (a) The initial site, (b) the saddle-point configuration, (c) the final site.

conjugated chain with a  $V_H$  that has migrated down the alkyl chain. This model appears to be consistent with the observation of the two different thermal annealing activation energies.

The calculated energy required to create a pair of defects, one  $CH_2$  defect on site 4 of one polymer together with a  $V_H(A1)$  on a second polymer, is 2.2 eV. This is significantly less than the expected cost in energy to break a C-H bond ( $\sim 4$  eV). Thus, if the C-H bond breaking occurs concurrently with bond forming it may be possible to create defects in a process requiring less than 4 eV.

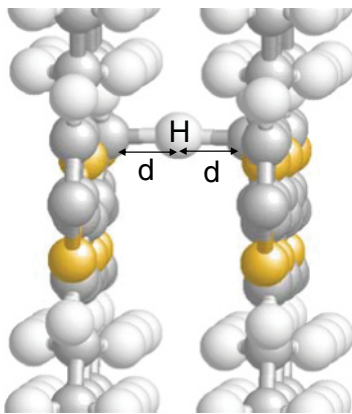


FIG. 17. (Color online) Migration of hydrogen between two P3AT polymers occurs with activation energy of 0.7 eV. The figure shows a saddle-point structure in which the migrating H atom is one-half the distance between the two polymers. At the saddle point, the C atoms are displaced out of the polymer plane by about 0.46 Å, and the C-H distance is stretched to  $d = 1.44$  Å.

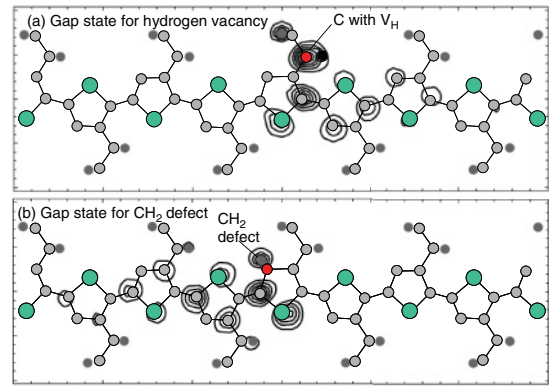


FIG. 18. (Color online) (a) Contour map of the wave function for the gap state associated with a  $V_H(A1)$  defect. (b) Contour map of the wave function for the gap state associated with a  $CH_2$  defect. Green (large) spheres indicate S atoms. Grey (small) spheres indicate C atoms. Black spheres indicate H atoms. The plane of the plot is 0.11 nm away from the plane of the backbone; therefore, the atomic positions have been projected onto this plane.

Calculations of the electronic structure for P3AT polymer chains containing one  $CH_2$  defect or one  $V_H$  defect in each supercell show clearly the presence of localized states in the band gap for both defects. Contour plots of the gap states for the two defects are shown in Fig. 18. The wave-function for the gap state arising from the  $V_H$  defect is localized mainly on the  $sp^2$  bonded C atom in the alkyl chain but also couples to the C and S atoms in the conjugated chain. The wave function for the gap state associated with the  $CH_2$  defect is localized near the defect and decays to zero over a distance of about three thiophene rings. The single particle energy level for the  $V_H$  defect calculated using the local density approximation is  $E_{vbm} + 0.22$  eV, where  $E_{vbm}$  is the energy of the valence band maximum. The corresponding level for the  $CH_2$  defect is  $E_{vbm} + 0.55$  eV. These energy levels were obtained by modeling the defects in ordered P3AT polymers, where the tilt angle of the conjugated backbone is equal to about  $23^\circ$  and an interpolymer  $\pi$ -stacking spacing is 3.8 Å.

## IV. DISCUSSION

### A. The low energy spectral shape

Figure 5 shows that the low energy band of the PCDTBT:PCBM spectral response cuts off at about 0.7–0.75 eV. In steady state, two sequential optical transitions involving deep trap states are necessary to generate a photocurrent—one transition creating a mobile electron in the fullerene and the other a mobile hole in the polymer. The interface band gap is known to be 1.4–1.45 eV,<sup>16</sup> and hence photon energies less than half the interface gap should not be able to generate a photocurrent. The cut-off in the low energy absorption at about 0.7 eV is therefore readily explained. For P3HT:PCBM, the interface gap is about 1.2 eV and so the threshold is expected near 0.6 eV, which is consistent with the data in Fig. 12. The spectrum is a convolution of the trap density of states distribution with the band edge density of states for the polymer and the fullerene plus possible phonon

sidebands. We cannot determine from the spectrum whether the trap state has a narrow or broad energy distribution.

It is also possible to generate photocurrent from trap-related transitions with both optical transitions within either the polymer or the PCBM, followed by migration of one or other carrier to the interface. Such transitions will have a higher energy threshold since the optical gap of either bulk material is larger than the interface band gap. These transitions may be present but will be hidden by the CT transitions because of their lower threshold energy, and at this point we cannot determine whether they contribute significantly to the spectra.

### B. Models for defect creation and annealing

The measurements show that x-ray irradiation introduces deep localized trap states in PCDTBT:PCBM, as indicated by the broad low energy band in the spectral response. These states act as recombination centers that reduce the cell fill factor and also increase the ideality factor of the dark current. The traps have the following properties:

(1) Recombination centers introduced by x-ray or light irradiation are indistinguishable electronically, and a smaller density of similar electronic states are present before either type of irradiation.

(2) The induced states are reversed by annealing to about 100 °C and are characterized by two different annealing rates that we associate with different thermal energies in the range 1–1.3 eV. The states that are present before irradiation do not anneal out.

(3) The annealing properties of x-ray induced and light induced states are significantly different. X-ray induced states anneal primarily with the faster time constant, while the light induced states anneal almost entirely with the slower time constant, and there are residual stable states.

(4) P3HT:PCBM also has radiation induced traps with similar electronic and annealing properties as PCDTBT:PCBM.

The structure calculations of Sec. III.B provide a natural general explanation for these specific properties. The abstraction of hydrogen from the polymer and its attachment elsewhere to the conjugated rings creates defects with electronic states in the band gap. Hydrogen migration can recover the initial state and is calculated to have a migration energy of 1.2–1.4 eV, in good agreement with experiment. The different migration energy along the conjugated rings (1.2 eV) and along the alkyl chain (1.4 eV) provide a plausible explanation for the fast and slow annealing rates.

The similarity of light induced and x-ray induced states lead us to propose that they have the same origin, i.e., hydrogen abstraction from the polymer. How a C-H bond can be broken with photons of relatively low energy has several possible answers. There may be enough intensity at about 4 eV in sunlight passing through the typical glass substrate to abstract hydrogen, perhaps with the help of some thermal energy. The creation of traps by a nominal white light photon is a rare event, which we estimate to be of order 1 in  $10^{10}$  photons from the light intensity and exposure duration. Hence a defect creation mechanism with low probability can still be effective in creating the trap states. Alternatively, the theoretical calculations show that only 2.2 eV is needed to create an adjacent defect pair comprising the  $V_H$  vacancy and the  $CH_2$

defect, which is well within the range of visible photons. The pair would need to be able to move apart to prevent the reverse process from annihilating the defects. A third possibility is that since optical excitation creates a population of valence band holes and conduction band electrons, further optical excitation of these carriers can generate enough total excitation energy to break a C-H bond and abstract hydrogen. Unlike the x-ray irradiation, light absorption only excites the  $\pi$ -bonded states of the conjugated rings and does not have enough energy to excite the alkyl chains. Hence a different population of hydrogen sites is affected, and this may be the origin of the different annealing properties. Experiments to measure the defect creation as a function of intensity and wavelength should provide further insight.

The measurements find that similar trap states are present before irradiation but do not anneal out. These states may be structurally different and more stable, even though they are not distinguishable electronically. A second possibility is that they are states in a structural thermal equilibrium and so are the minimum number of states that can be attained at the anneal temperature.

Other types of defect states need to be considered, the most obvious being states associated with impurities and with the fullerenes. UV damage to polymers often occurs through an oxygen reaction,<sup>44</sup> for example, forming carbonyl units. The role of oxygen in these samples cannot be excluded, since it is almost certainly present at some level despite the encapsulation and storage in nitrogen. However, the relatively low energy of the thermal recovery argues against such a tightly bound defect state. Furthermore, the estimate that a secondary electron-hole pair has a  $\sim 1\%$  chance of creating a defect also implies that it is unlikely that defect formation by x-ray radiation is associated with impurities such as  $O_2$  or  $H_2O$ . The high energy secondary electron-hole pair loses energy very rapidly and will not retain enough energy to break a bond after it migrates just a few atomic distances. Hence, even if the cell contains as much as 1% impurities, the secondary electron-hole pair would have to create an impurity-related defect with  $\sim 100\%$  probability, which seems unlikely. Hence we think that most of the defects formed by x-ray irradiation are not associated with impurities. However, the traps present before irradiation could be impurity related.

Fullerenes can be easily and reversibly hydrogenated.<sup>45,46</sup> Hence hydrogen abstracted from the polymer or from the PCBM could migrate and attach to the fullerene cage. The resulting C-H bond breaks the conjugation of the fullerene and probably introduces deep traps. Hydrogen that migrates from the polymer will preferentially bond to the fullerenes near the heterojunction interface, putting it in the optimum position to form a recombination center.

In summary, the evidence is strong that hydrogen abstraction is the origin of x-ray radiation induced electronic defects and that thermally activated hydrogen migration is the mechanism of annealing. The evidence suggests that this mechanism also applies to light induced defects. However, there are alternative specific models for both the defect state and the annealing pathways so that we cannot be sure of the details. Techniques such as photocurrent-detected magnetic resonance may provide structural identification, and the role of the fullerenes and impurities also needs to be clarified.

### C. Properties of traps and recombination centers

The capture cross section of the radiation induced recombination centers can be estimated from the photocurrent measurements of mobility-lifetime product. The 276 hour exposure data in Fig. 2 yields  $\mu\tau \sim 10^{-10} \text{ cm}^2\text{V}^{-1}$  from the fit of the  $J_{\text{PC}}(V)$  data and corresponds to the estimated  $N_{\text{R}} = 1-2 \times 10^{16} \text{ cm}^{-3}$ . For a hopping system the constant in (1) is  $ea/6kT \cong 2 \times 10^{-7}$ ,<sup>47</sup> where  $a$  is the hopping length set equal to 0.3 nm, from which the capture cross section is about  $10^{-13} \text{ cm}^2$ , which is a surprisingly large value. Possibly the defect density estimate is too low, but we point out that the cross section could be enhanced by the molecular nature of the polymer. A carrier can move easily along the conjugated polymer backbone but hops more slowly between molecules. Hence the carrier is likely to be trapped in a molecule that contains a defect, irrespective of the arrival hopping site. Consequently, the capture cross-section reflects the apparent size of the molecule rather than the effective size of the defect. A long polymer chain is therefore consistent with a high capture cross-section. Small molecule organic solar cells could have an advantage of a smaller effective trap capture cross section simply based on the molecule size.

Midgap defect states only act as recombination centers if they are sufficiently close to the heterojunction interface to interact with both electrons in the fullerene conduction band and holes in the polymer valence band. Sustained photocurrent with low energy excitation results from the step-wise excitation of an electron from the polymer valence band to a localized trap state together with excitation from the trap to the fullerene conduction band. For the case that both transitions occur by optical excitation, the first of these transitions is denoted by a rate  $G\alpha_{\text{P}}(x)$  and the second by  $G\alpha_{\text{F}}(x)$ , where  $x$  is the distance of the trap state from the heterojunction interface, and  $G$  is the incident light flux. The electron occupancy of the trap is denoted by  $P_{\text{E}}(x)$ . For simplicity we only consider trap states of density  $N(x)$  within the polymer, but there is an equivalent contribution from traps in the fullerene domain. Steady state excitation implies equal excitation rates for the two transitions at each trap state, so that

$$G\alpha_{\text{F}}(x)N(x)P_{\text{E}}(x) = G\alpha_{\text{P}}(x)N(x)[1 - P_{\text{E}}(x)] + \text{thermal exc.} - \text{hole capture.} \quad (4)$$

The photocurrent is proportional to the integral over  $x$ . The two extra terms on the right side recognize that the transition between the polymer valence band and the trap could be by thermal excitation of holes to the band edge or by capture of free holes depending on the circumstances, as explained shortly. The model is illustrated in Fig. 19.

Considering only the optical transitions, the transition rate to the fullerene decreases rapidly away from the interface since it involves tunneling the distance  $x$ , hence,

$$\alpha_{\text{F}}(x) = \alpha_{\text{F0}} \exp(-2x/R_{\text{T}}), \quad (5)$$

where  $R_{\text{T}}$  is a characteristic tunneling length. The optical transitions from the polymer valence band to the trap do not involve tunneling, so that  $\alpha_{\text{P}}(x) = \alpha_{\text{P0}}$ . The result is that  $\alpha_{\text{F}}(x) \rightarrow 0$  when  $x$  is larger than a few multiples of  $R_{\text{T}}$ . Hence, according to Eq. (4),  $P_{\text{E}}(x) \rightarrow 1$ , and the traps away from the interface are fully occupied by electrons. For these distant

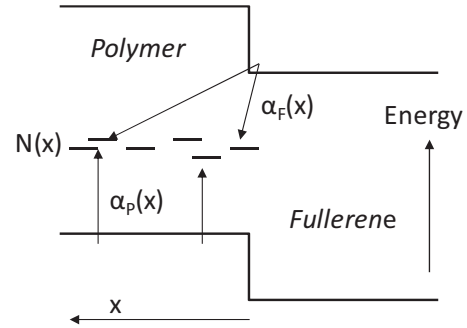


FIG. 19. Band diagram of PCDTBT:PCBM heterojunction showing the optical transitions through deep localized states, as described in the text.

states at  $x \gg R_{\text{T}}$ , the transition rates on either side of Eq. (4) are zero and there is no contribution to the photocurrent. This analysis confirms that the recombination centers must be close to the interface within a distance of about  $R_{\text{T}}$ , and that two optical excitations are required to create one electron-hole pair. The measured spectral response is the sum of the two optical transitions, but these cannot be distinguished in the data of Figs. 1 or 5. At any excitation energy, the two transitions must have equal rates to maintain a steady state, and the equal rates are maintained by the occupancy factor  $P_{\text{E}}(x)$ . The incident illumination is about  $500 \mu\text{W}/\text{cm}^2$  ( $\sim 3 \times 10^{15}$  photons/ $\text{cm}^2$ ), and from the data in Fig. 1 the measured trap absorption is about  $10^{-5}$  at 1 eV, so that (4) gives  $\alpha_{\text{P0}} \sim 10 \text{ s}^{-1}$  for the estimated  $1-2 \times 10^{16} \text{ cm}^{-3}$  density of recombination centers.

Next we include the effect of thermal excitation. The optical excitation of an electron from a trap to the fullerene side of the interface leaves a trapped hole. Instead of an optical transition, the hole could be thermally excited to the polymer valence band with rate  $\omega_0 \exp(-E_{\text{T}}/kT)$ , where  $E_{\text{T}}$  is the trap depth and  $\omega_0$  is the usual prefactor of order  $10^{12} \text{ s}^{-1}$ . The thermal excitation rate is larger than the optical excitation rate when the trap depth is small enough and the crossover in rates occurs at a trap depth  $E_{\text{TX}}$  given by

$$\alpha_0 = \omega_0 \exp(-E_{\text{TX}}/kT); E_{\text{TX}} = kT \ln(\omega_0/\alpha_0). \quad (6)$$

Inserting values for  $\omega_0$  and  $\alpha_0$  shows that trapping states that are shallower than 0.6 eV will be repopulated thermally at room temperature, while deeper traps can only be repopulated optically. The band tail states that are the origin of the spectral response in the energy range 1.1–1.4 eV are sufficiently shallow to be repopulated thermally, and hence only a single optical excitation of these states creates an electron-hole pair.

Bias light changes the situation again. The bias illumination creates a large density of mobile electrons in the fullerene and holes in the polymer. The holes are readily captured into the traps that are fully occupied by electrons. The trap occupancy  $P_{\text{E}}(x)$  changes and therefore also the absorption characteristics. In particular, away from the interface, where  $P_{\text{E}}(x > R_{\text{T}}) = 1$  in the absence of bias light, the valence band holes will repopulate these traps with holes so that  $P_{\text{E}}(x) < 1$ . The optical transitions corresponding to the broad band at 0.8–1.1 eV can now excite these holes, and hence many more trap state optical excitations can contribute to 1 eV

photocurrent rather than only those near the heterojunction interface. This mechanism accounts for the large enhancement of the photocurrent under bias light illumination. The absence of a bias light effect for the band tail region of the spectral response and the small effect in P3HT:PCBM is because the states involved are sufficiently shallow to be repopulated thermally so that the bias light does not significantly change the occupancy.

## V. CONCLUSIONS

X-ray exposure of PCDTBT:PCBM BHJ solar cells results in the creation of deep trap states that act as recombination centers, and the states are observed by an increase in the low energy photocurrent spectral response. The induced states are reversible by annealing with two distinctly different time constants, reflecting an anneal energy of 1–1.2 eV, while the states that are present before irradiation do not anneal away. Hence the data indicate three different types of annealing processes, although the localized states are indistinguishable electrically. Analysis of the x-ray irradiation and theoretical modeling suggest that hydrogen abstraction from C-H bonds is the primary mechanism of defect formation. The resulting gap state and hydrogen migration energy are consistent with

the spectral response and the annealing data. There are several alternative bonding sites for the abstracted hydrogen and also alternative annealing pathways, which could account for the different processes. However, we cannot yet positively identify the specific defect structure from the available alternatives. Prolonged white light exposure creates similar thermally reversible recombination centers from which we conclude that the basic defect creation mechanism is similar to x-ray irradiation. However the significantly different annealing kinetics suggests a modified defect recovery pathway.

Although significant degradation of the cells occur with x-ray exposure, the effect is relatively small and should not be a significant problem for normal use of medical x-ray detectors, which typically need to withstand up to 1000 Gy. However, further studies of x-ray effects at clinical x-ray energies is needed.

## ACKNOWLEDGMENTS

The authors are grateful to A. Heeger and S. Cowan for providing the solar cell samples, to G. Whiting for helpful discussion, and to A. Krakaris and C. Paulson for technical assistance. This work was supported in part by the AFOSR under Grant No. FA9550-09-1-0436.

\*street@parc.com

- <sup>1</sup>J. A. Hauch, P. Schilinsky, S. A. Choulis, R. Childers, M. Biele, and C. J. Brabec, *Solar Energy Materials and Solar Cells* **92**, 727 (2008).
- <sup>2</sup>C. H. Peters, I. T. Sachs-Quintana, W. R. Mateker, T. Heumueller, J. Rivnay, R. Noriega, Z. M. Beiley, E. T. Hoke, A. Salleo, and M. McGehee, *Adv. Mater.* **24**, 663 (2012).
- <sup>3</sup>K. Kawano and C. Adachi, *Adv. Funct. Mater.* **19**, 3934 (2009).
- <sup>4</sup>M. Manceau, A. Rivaton, J-L Gardette, S. Guillerez, and N. Lemaitre, *Solar Energy Materials and Solar Cells* **95**, 1315 (2011).
- <sup>5</sup>K. Kawano and C. Adachi, *Appl. Phys. Lett.* **96**, 053307 (2010).
- <sup>6</sup>M. O. Reese, A. M. Nardes, B. L. Rupert, R. E. Larsen, D. C. Olson, M. T. Lloyd, S. E. Shaheen, D. S. Ginley, G. Rumbles, and N. Kopidakis, *Adv. Funct. Mater.* **20**, 3476 (2010).
- <sup>7</sup>K. Lee, J. Y. Kim, S. H. Park, S. H. Kim, S. Cho, and A. J. Heeger, *Adv. Mater.* **19**, 2445 (2007).
- <sup>8</sup>Y. Sun, C. J. Takacs, S. R. Cowan, J. H. Seo, X. Gong, A. Roy, and A. J. Heeger, *Adv. Mater.* **23**, 2226 (2011).
- <sup>9</sup>M. Roberts, K. Asada, M. Cass, C. Coward, S. King, A. Lee, M. Pintani, M. Ramon, and C. Foden, *SPIE Conf. Proc.* **7722**, (2010).
- <sup>10</sup>P. Kobrin, R. Fisher, and A. Gurrola, *Appl. Phys. Lett.* **85**, 2385 (2004).
- <sup>11</sup>R. A. Street, A. Krakaris, and S. R. Cowan, *Adv. Funct. Mater.* (in press).
- <sup>12</sup>P. Schilinsky, C. Waldauf, and C. J. Brabec, *Appl. Phys. Lett.* **81**, 3885 (2002).
- <sup>13</sup>F. A. Boroumand, M. Zhu, A. B. Dalton, J. L. Keddie, P. J. Sellin, and P. J. Sellin, *Appl. Phys. Lett.* **91**, 033509 (2007).
- <sup>14</sup>P. E. Keivanidis, N. C. Greenham, H. Siringhaus, R. H. Friend, J. C. Blakesley, R. Speller, M. Campoy-Quiles, T. Agostinelli, D. D. C. Bradley, and J. Nelson, *Appl. Phys. Lett.* **92**, 023304 (2008).

- <sup>15</sup>J. W. Kingsley, S. J. Weston, and D. G. Lidzey, *IEEE JSTQE* **16**, 1770 (2010).
- <sup>16</sup>R. A. Street, K. W. Song, J. E. Northrup, and S. Cowan, *Phys. Rev. B* **83**, 165207 (2011).
- <sup>17</sup>L. Goris, A. Poruba, L. Hodakova, M. Vanacek, K. Haenen, M. Nesladek, P. Wagner, D. Vandezande, L. De Schepper, and J. V. Manca, *Appl. Phys. Lett.* **88**, 052113 (2006).
- <sup>18</sup>N. Blouin, A. Michaud, and M. Leclerc, *Adv. Mater.* **19**, 2295 (2007).
- <sup>19</sup>M. Tong, N. E. Coates, D. Moses, A. J. Heeger, S. Beaupre, and M. Leclerc, *Phys. Rev. B* **81**, 125210 (2010).
- <sup>20</sup>S. R. Cowan, W. L. Leong, N. Banerji, G. Dennier, and A. J. Heeger, *Adv. Funct. Mater.* **21**, 3083 (2011).
- <sup>21</sup>S. H. Park, A. Roy, S. Beaupre, S. Cho, N. Coates, J. S. Moon, D. Moses, M. Leclerc, K. Lee, and A. J. Heeger, *Nat. Photonics* **3**, 297 (2009).
- <sup>22</sup>R. A. Street, *Proc. SPIE* 8098 (2011).
- <sup>23</sup>J. Lee, K. Vandewal, S. R. Yost, M. E. Bahlke, L. Goris, M. A. Baldo, J. V. Manca, and T. Van Voorhis, *J. Am. Chem. Soc.* **132**, 11878 (2010).
- <sup>24</sup>K. Vandewal, K. Tvingstedt, A. Gadisa, O. Inganäs, and J. V. Manca, *Phys. Rev. B* **81**, 125204 (2010).
- <sup>25</sup>C. G. Shuttle, N. D. Treat, J. D. Douglas, J. M. J. Frechet, and M. L. Chabiny, *Adv. Energy Mater.* **2**, 111 (2011).
- <sup>26</sup>L. Tzabari and N. Tessler, *J. Appl. Phys.* **109**, 064501 (2011).
- <sup>27</sup>D. Ray, L. Burtone, K. Leo, and M. Riede, *Phys. Rev. B* **82**, 125204 (2010).
- <sup>28</sup>J. D. Servantes, S. Yeganeh, T. J. Marks, and M. A. Ratner, *Adv. Funct. Mater.* **20**, 97 (2010).
- <sup>29</sup>R. A. Street, K. W. Song, and S. Cowan, *Org. Electronics* **12**, 244 (2011).

- <sup>30</sup>R. A. Street, M. Schoendorf, A. Roy, and J. H. Lee, *Phys. Rev. B* **81**, 205307 (2010).
- <sup>31</sup>J. H. Lee, S. Cho, A. Roy, H-T Jung, and A. J. Heeger, *Appl. Phys. Lett.* **96**, 163303 (2010).
- <sup>32</sup>N. C. Giebink, G. P. Wiederrecht, M. R. Wasielewski, and S. R. Forrest, *Phys. Rev. B* **82**, 155305 (2010).
- <sup>33</sup>R. A. Street and M. Hack, *MRS Symp. Proc.* **219**, 135 (1991).
- <sup>34</sup>H. Ahn, D. W. Oblas, and J. E. Witten, *Macromolecules* **37**, 3381 (2004).
- <sup>35</sup>L-L. Chua, M. Dipankar, S. Sivaramakrishnan, X. Gao, D. Qi, A. T. S. Wee, and P. K. H. Ho, *Langmuir* **22**, 8587 (2006).
- <sup>36</sup>F. Bebensee, J. Zhu, J. H. Baricuatro, J. A. Farmer, Y. Bai, H-P. Steinruck, C. T. Campbell, and J. M. Gottfried, *Langmuir* **26**, 9632 (2010).
- <sup>37</sup>R. F. Egerton and M. Takeuchi, *Appl. Phys. Lett.* **75**, 1884 (1999).
- <sup>38</sup>R. A. Street, *Phys. Rev. B* **84**, 075208 (2011).
- <sup>39</sup>W. Kohn and L. J. Sham, *Phys. Rev.* **140**, 1133 (1965).
- <sup>40</sup>M. Bockstedte, A. Kley, J. Neugebauer, and M. Scheffler, *Comput. Phys. Commun.* **107**, 187 (1997).
- <sup>41</sup>N. Troullier and J. L. Martins, *Phys. Rev. B* **43**, 1993 (1991).
- <sup>42</sup>J. E. Northrup, *Appl. Phys. Lett.* **99**, 062111 (2011).
- <sup>43</sup>J. E. Northrup and M. L. Chabinyc, *Phys. Rev. B* **68**, 041202 (2003).
- <sup>44</sup>A. L. Andradý, S. H. Hamid, Z. X. Hu, and A. Torikai, *J. Photochem. Photobiol., B* **46**, 96 (1998).
- <sup>45</sup>C. Jin, R. Hettich, R. Compton, D. Joyce, J. Blencoe, and T. Burch, *J. Phys. Chem. Solids* **98**, 4215 (1994).
- <sup>46</sup>V. Y. Davydov, N. Sheppard, and E. Osawa, *J. Catal.* **211**, 42 (2002).
- <sup>47</sup>R. A. Street, *Philos. Mag.* **49**, L15 (1984).